# Modeling and Control of a Novel Hybrid Ground Aerial Robot

Mahmoud Elsamanty[1], Mohamed Fanni[2], Ahmed Ramadan[3], Ahmed Abo-Ismail[4]

[1,4] *Mechatronics and Robotics Eng. Dept., Egypt-Japan University of Science and Technology, Alexandria, Egypt*
[2]*Adjunct Professor at Mechatronics and Robotics Eng. Dept., Egypt-Japan University of Science and Technology.*
*Prod. Eng. & Mechanical Design Dept., Mansoura University, Mansoura, Egypt.*
[3]*Adjunct Professor at Mechatronics and Robotics Eng. Dept., Egypt-Japan University of Science and Technology.*
*Computers Engineering & Automatic Control Dept., Tanta University, Tanta, Egypt.*
mahmoud.elsamanty@ejust.edu.eg, mfanni@mans.edu.eg, ahmed.ramadan@ejust.edu.eg,
aboismail@ejust.edu.eg

*Abstract* – **This paper presents the dynamic modeling and control simulation of a novel robot that combines flying motion and on ground motion into an integrated single robot. The ground motion is based on four wheels configuration that provides more stability. The flying motion is depending on the flying mechanism of quadrotor system. Smart transformation mechanism is developed to switch the robot from the ground motion configuration to the flying motion configuration and vice versa without adding any additional actuators. A manipulator with 3 DOF is added to handle an object during the ground motion and it is useful to hold this object during the flying motion. A CAD model is developed using SOLIDWORKS. The dynamic model of this robot is derived to achieve the eccentricity of the payload, the weight of the eccentric manipulator and managing the variation of the payload in the dynamic model. The derived robot dynamics are highly nonlinear. A controller is designed based on feedback linearization technique to stabilize the robot attitude and altitude. Controlling the horizontal movements' nonholonomic constraints is used to generate the desired trajectories of robot attitudes. Another dynamic model and controller have been established for the transformation mechanism. Finally, the simulation results using MATLAB/SIMULINK show that the controller successfully vanish the eccentric effect and stabilize the robot attitude.**

*Keywords* – *Flying robot; Dynamic Modeling of UAV; Feedback Linearization technique; Controller design.*

## I. INTRODUCTION

Ground Mobile Robots (GMR) and Unmanned Aerial Vehicles (UAV) have great improvements nowadays due to their applications. GMR applications are dealing with area that has enormous dangers for human life [1, 2]. The most amazing applications are Service robots, patrolling large areas whether indoor or outdoor and map exploration. GMR also can be used in land mining, searching operation for victims after the earthquake, or in collapsed buildings which can minimize the risks for rescuers. For the UAVs, it has a lot of applications like land security and surveillance, military operations, monitoring the civilian operations like in large construction sites, and forest fire fighting [3 – 5]. The mission for both two types is reporting the location of victims, or target acquisition in case of surveillance. But each of the two types has its own difficulties. For GMRs moving over terrain or in unstructured area is a great drawback and losing the communication signal is another problem in exploring the unreachable areas. For UAVs, drawbacks can be listed as: its small payload, small flying time. All the previous drawbacks for GMRs and UAVs were the motivation to develop a new robot that combines the two capabilities into one integrated robot to overcome – as much as possible - these difficulties. The new robot can be used in rescue operation, surveillance, construction operations, firefighting, mining accidents, or in closed places full of poisonous substances (gas, radiation...).

Recently, UAVs have attracted an extensive research work. Some of these UAVs research are concentrated on the design [6 – 8]; others are concerned with the stabilizing, hovering and aerial obstacles avoidance [9 – 14]. Complete dynamic model has been presented in details [11, 13 and 15]. New research area of aerial manipulation has been developed using UAVs [17, 18]. In the previous work [16] a complete design is developed to withstand all the external forces. A CAD model is constructed and tested using the finite element method in ANSYS 14. Besides, control hardware was selected based on the design results

In this research a complete conceptual design is presented. The main design is to combine the flying motion using the quadrotor basis to the ground motion platform to generate an integrated robot that can maneuver in ground and on the sky. The design describes also a transformation mechanism that used to switch the rotor arms from the horizontal direction to the vertical direction and vice versa. This mechanism is dynamically modeled and controlled. A complete dynamic model for the Hybrid Aerial ground robot "HGAR" is presented in details. After modeling HGAR, a controller is designed based on the feedback linearization method in order to stabilize the attitude and altitude.

This paper presents the design of a novel robot that combine the capabilities of flying motion and on ground motion. Section II describes the whole robot conceptual design for the ground platform, flying platform, and transformation mechanism. Section III presents a complete description for extracting the physical model parameters, deriving the applied moment and forces, and deriving the dynamic model for the new robot in the flying motion only as it is more challenging.

The controller design based on feedback linearization technique is presented in Section IV. Section V describes the transformation mechanism dynamic model and its controller design. The simulation results using MATLAB/SIMULINK are presented in Section VI. Finally conclusions and future work are presented in Section VII.

## II. ROBOT CONCEPTUAL DESIGN

### A. Ground platform

The design of the ground platform is based on a four wheel type [11], which provides more stability in landing as well as in ground motion. The arrangement of these wheels is consisting of two motorized standard wheels, and two free caster wheels of normal or omnidirectional type as shown in Fig.1. Each wheel is assembled to a rigid bracket which is connected directly to the base of the robot structure using four bolts. This bracket is designed to maintain the wheel's DC motor inside its frame. To ensure the rigidity of the bracket frame, four cylindrical ribs are installed inside the frame. One of these ribs will be used to support motor from the lower side. Large distance between each two opposite wheels gives the robot more stability during ground motion and gives the ability to move over small rough surface. The two motorized standard wheels will simplify the control of the ground motion. Although more motorized wheels increase the maneuverability, they increase the weight of the platform which is not recommended in this design.
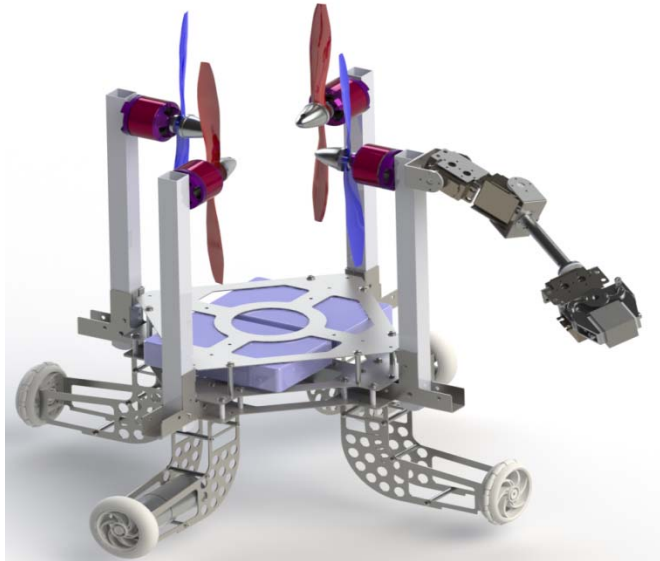


Figure 1. MOBILE GROUND PLATFORM CONFIGURATION

### B. Flying platform

The flying platform is designed on the basis of quadrotor platform, which is the best choice for the flying platform of the proposed HGAR robot as presented in the previous work [16]. The flying platform was designed to support the weight of HGAR structure, batteries, electronic boards and all the auxiliary components. Fig.2 presents the proposed flying platform, which consists of four rotors installed on four arms. These arms have square hollow cross sections and are made from Aluminum alloy to ensure rigidity and light weight. Each arm is pivoted at its end to give the arm the flexibility to rotate about a horizontal axis relative to the platform as requested by the design of transformation mechanism.

### C. Transformation mechanism

The main objective of the transformation mechanism is to reduce the lateral space occupied by the HGAR robot when it is in ground motion mode to improve the robot maneuverability in confined spaces. Raising the arms which carry the propellers to the vertical position will realize this objective as showing in Fig.3. The working principle of the transformation mechanism is unlocking the solenoids of the securing mechanisms, and then the arms will be free to rotate about the pivot pins. The controlled thrust force resulted from the propeller will generate a moment about the pivot pin which forces the arm to rotate about the pivot pin, and becomes in the vertical direction. After the arm reaches to the vertical position, the propeller rotation will be stopped and the solenoids will secure the arm again to the pivot support and prevent it from any movements. The sequence of arms' motion is that each two opposite arms will be rising up at the same time and after reaching to the vertical position, the other two arms will start motion until reaching to the vertical position. Also the propeller blades are provided by a controller to put them in the vertical position as shown in Fig.1. A serial manipulator [17, 18] with 3-DOF is added to the robot at one specific arm. This manipulator is activated during the ground motion mode. A gripper is attached to the manipulator end; all of the manipulator three joints are revolute joints.
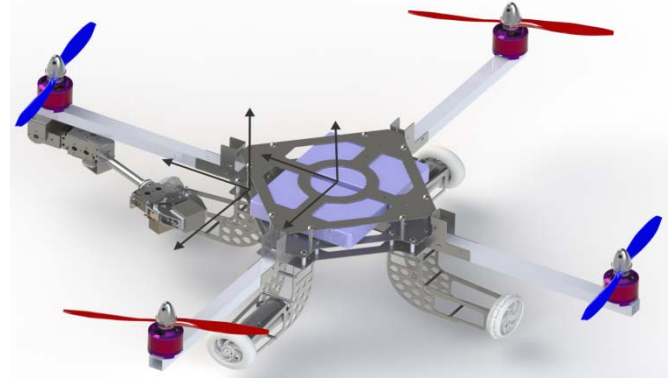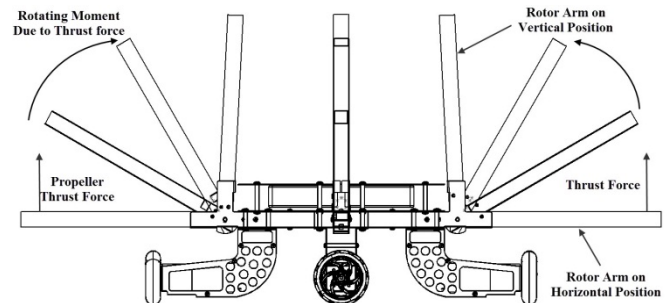


Figure 2. FLYING PLSTFORM CONFIGURATION



Figure 3. CLOSING MOTION OF TRANSFORMATION MECHANISM

## III. DYNAMIC MODEL OF HGAR

The model of HGAR can be described as two independent subsystems, which are flying motion configuration and ground motion configuration. For the flying configuration, it is described as a 6-DOF platform, while it wil be of 3-DOF during the ground motion configuration. In this paper, the dynamic model for the HGAR is derived for the flying configuration only which is dealing with the eccentricity of the center of gravity and the change of payload.

### A. System Physical parameters

A CAD model as shown in fig.1 and fig.2 is developed using SOLIDWORKS. The modeled parts are the brushless DC motors, propellers, batteries, Aluminum frames, and wheels. The total mass, center of gravity position and mass moment of inertia of the HGAR robot is calculated by the aid of the CAD model. Table I presents all the physical parameters of the HGAR robot without adding the effect of the payload. It is noticed that the inertia matrix is square non symmetric. This is because the center of gravity shifted a distances Xcg, Ycg and Zcg away from the geometric center.

TABLE I

SYSTEM PARAMETERS

| Para. | Value | Unit | Para. | Value | Unit |
|-------|-------|------|-------|-------|------|
| $X_{cg}$ | 31.43 | mm | $I_r$ | $4.5\times10^{-5}$ | kg.m$^2$ |
| $Y_{cg}$ | 0.55 | mm | $m_R$ | 3.653 | kg |
| $Z_{cg}$ | -0.95 | mm | $L$ | 0.4116 | m |
| $I_{xx}$ | $9.281\times10^{-2}$ | kg.m$^2$ | $g$ | 9.8 | m.s$^{-2}$ |
| $I_{xy}$ | $-3.435\times10^{-3}$ | kg.m$^2$ | $K_{t1}$ | $1.08\times10^{-3}$ | kg.s$^2$.rad$^{-2}$ |
| $I_{xz}$ | $-7.463\times10^{-4}$ | kg.m$^2$ | $K_{t2}$ | $1.08\times10^{-3}$ | kg.s$^2$.rad$^{-2}$ |
| $I_{yx}$ | $-7.463\times10^{-4}$ | kg.m$^2$ | $K_{t3}$ | $1.08\times10^{-3}$ | kg.s$^2$.rad$^{-2}$ |
| $I_{yy}$ | $1.838\times10^{-1}$ | kg.m$^2$ | $K_{t4}$ | $1.08\times10^{-3}$ | kg.s$^2$.rad$^{-2}$ |
| $I_{yz}$ | $1.164\times10^{-4}$ | kg.m$^2$ | $K_{d1}$ | $2.09\times10^{-7}$ | kg.m.s$^2$.rad$^{-2}$ |
| $I_{zx}$ | $1.164\times10^{-4}$ | kg.m$^2$ | $K_{d2}$ | $2.09\times10^{-7}$ | kg.m.s$^2$.rad$^{-2}$ |
| $I_{zy}$ | $1.164\times10^{-4}$ | kg.m$^2$ | $K_{d3}$ | $2.09\times10^{-7}$ | kg.m.s$^2$.rad$^{-2}$ |
| $I_{zz}$ | $1.115\times10^{-1}$ | kg.m$^2$ | $K_{d4}$ | $2.09\times10^{-7}$ | kg.m.s$^2$.rad$^{-2}$ |

Second stage is studying the effect of changing the mass of payload $m_l$ on the physical parameters of the HGAR. This study is done by attaching a mass to the gripper and holding the manipulator in its home position. This mass is varied from 0 to 250 gram and extracting the mass moments of inertia from the CAD model according to the change of the mass. This data is collected and then a curve fitting procedures is performed to obtain a direct relation between the changes of the mass and all the physical parameters. Equations (1) to (12) are defining the mentioned relationships. It is a high order polynomial equation and its parameters $p_1$, $p_2$, $p_3$, $p_4$ and $p_5$ are presented in Table II.

$$X_{cg} = p_{x1}m_l^3 + p_{x2}m_l^2 + p_{x3}m_l + p_{x4} \tag{1}$$

$$Y_{cg} = p_{y1}m_l^3 + p_{y2}m_l^2 + p_{y3}m_l + p_{y4} \tag{2}$$

$$Z_{cg} = p_{z1}m_l^4 + p_{z2}m_l^3 + p_{z3}m_l^2 + p_{z4}m_l + p_{z5} \tag{3}$$

$$I_{xx} = p_{xx1}m_l^3 + p_{xx2}m_l^2 + p_{xx3}m_l + p_{xx4} \tag{4}$$

$$I_{xy} = p_{xy1}m_l^3 + p_{xy2}m_l^2 + p_{xy3}m_l + p_{xy4} \tag{5}$$

$$I_{xz} = p_{xz1}m_l^4 + p_{xz2}m_l^3 + p_{xz3}m_l^2 + p_{xz4}m_l + p_{xz5} \tag{6}$$

$$I_{yx} = p_{yx1}m_l^3 + p_{yx2}m_l^2 + p_{yx3}m_l + p_{yx4} \tag{7}$$

$$I_{yy} = p_{yy1}m_l^3 + p_{yy2}m_l^2 + p_{yy3}m_l + p_{yy4} \tag{8}$$

$$I_{yz} = p_{yz1}m_l^4 + p_{yz2}m_l^3 + p_{yz3}m_l^2 + p_{yz4}m_l + p_{yz5} \tag{9}$$

$$I_{zx} = p_{zx1}m_l^4 + p_{zx2}m_l^3 + p_{zx3}m_l^2 + p_{zx4}m_l + p_{zx5} \tag{10}$$

$$I_{zy} = p_{zy1}m_l^4 + p_{zy2}m_l^3 + p_{zy3}m_l^2 + p_{zy4}m_l + p_{zy5} \tag{11}$$

$$I_{zz} = p_{zz1}m_l^3 + p_{zz2}m_l^2 + p_{zz3}m_l + p_{zz4} \tag{12}$$

TABLE II

CURVE FITTING PARAMETERS

| Para | $p_1$ | $p_2$ | $p_3$ | $p_4$ | $p_5$ |
|------|-------|-------|-------|-------|-------|
| $X_{cg}$ | $7.05\times10^{-8}$ | $-3.8\times10^{-5}$ | 0.035 | 31.43 | |
| $Y_{cg}$ | $-6.9\times10^{-11}$ | $1.7\times10^{-6}$ | -0.0071 | 0.55 | |
| $Z_{cg}$ | $5.4\times10^{-10}$ | $-1.8\times10^{-7}$ | $7.9\times10^{-6}$ | $-9.1\times10^{-6}$ | -0.9502 |
| $I_{xx}$ | -0.0024 | 1.445 | 689 | $9.2\times10^{7}$ | |
| $I_{xy}$ | -0.0068 | 3.715 | -3453 | $-3.4\times10^{6}$ | |
| $I_{xz}$ | 0.000218 | -0.0664 | 0.838 | -249.2 | $-7.4\times10^{5}$ |
| $I_{yx}$ | -0.00682 | 3.715 | -3453 | $-3.4\times10^{6}$ | |
| $I_{yy}$ | 0.0554 | -27.19 | $1.6\times10^{4}$ | $1.8\times10^{8}$ | |
| $I_{yz}$ | $-5.3\times10^{-5}$ | 0.0169 | -0.419 | 59.59 | $1.1\times10^{5}$ |
| $I_{zx}$ | 0.000218 | -0.0664 | 0.838 | -249.2 | $-7.4\times10^{5}$ |
| $I_{zy}$ | $-5.3\times10^{-5}$ | 0.0169 | -0.419 | 59.59 | $1.1\times10^{5}$ |
| $I_{zz}$ | 0.062 | -29.87 | $1.7\times10^{4}$ | $1.1\times10^{8}$ | |

### B. General moments and forces

In this section all forces and moments applied to HGAR are presented. Some important assumptions are proposed to reach the applied forces and moments, then completing the dynamic model. First the HGAR structure is rigid enough to withstand the external forces during flying and on ground motion modes [16]. Second assumption; assuming that the body frame {B}, $O_b$ –xyz is coincident to the shifted center of mass (CM) to accomplish the dynamic model and simplifying the equations of motion rather than to be expressed in the geometrical center (GC). Final assumption; the earth frame {E}, $O_I$ –XYZ, is where position and orientation of the body frame is described with respect to it.

Let's define the rotation matrix $R_I^B$ which expresses the transformation from the inertial frame to the body frame. Fig.4 presents the angular velocity of the rotor i, denoted with $\omega_i$ that deliver a thrust force $T_i$. Based on the concept of the aerodynamics; the thrust force is directly proportional to the square angular velocity of the propeller. As a result of increasing the angular velocity, it leads to increase the drag resistance $\tau_{Mi}$. Finally the power consumed by the motor is calculated from the multiplication of this drag moment resistance times the angular velocity of the propeller.

$$R_I^B = \begin{bmatrix} c(\psi)c(\theta) & s(\psi)c(\theta) & -s(\theta) \\ -s(\psi)c(\phi)+c(\psi)s(\theta)s(\phi) & c(\psi)c(\phi)+s(\psi)s(\theta)s(\phi) & c(\theta)s(\phi) \\ s(\psi)s(\phi)+c(\psi)s(\theta)c(\phi) & -c(\psi)s(\phi)+s(\psi)s(\theta)c(\phi) & c(\theta)c(\phi) \end{bmatrix} \tag{13}$$

$$T_i = C_T\rho A(\omega_i R)^2 \tag{14}$$

$$\tau_{Mi} = C_Q\rho A(\omega_i R)^2 R \tag{15}$$

$$P_i = \tau_{Mi}\omega_i = C_Q \rho A(\omega_i R)^3 \qquad (16)$$

Where $C_T$ and $C_Q$ are the thrust force and drag moment coefficients respectively. These coefficients are depending on the propeller geometry, $\rho$ is the density of the air; A denotes the propeller surface area and finally the propeller radius R. after simplifying the previous equations it becomes as follows:

$$T_i = K_{ti}\omega_i^2 \qquad (17)$$
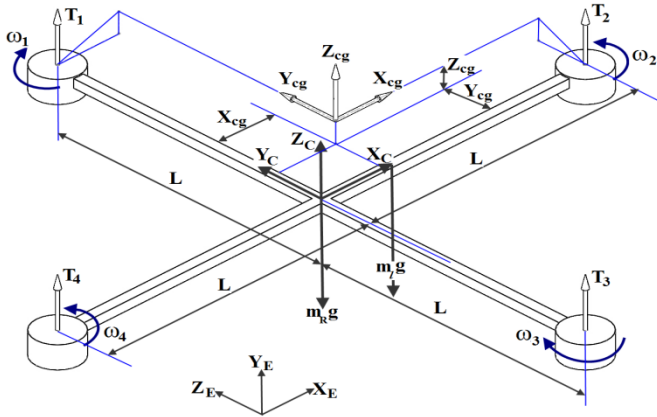
$$\tau_{Mi} = K_d \omega_i^2 \qquad (18)$$



Figure 4. SCHEMATIC DIAGRAM FOR THE HGAR FORCES AND COORDINATES

The summation of all the rotors thrust force is $T^B$ in $z$-axis and expressed in the body frame. Moments which applied to the HGAR during the flying are defined as $\tau_\phi$, $\tau_\theta$ and $\tau_\psi$. These moments are the rolling, pitching, yawing moment about the corresponding body frame xyz respectively. The shift of center of gravity affects the rolling and pitch moments due to the differences between the rotors angular speeds and distances between each rotor thrust force and the CM. The center of gravity shift does not affect the yawing moment, so yawing moment is appeared independent.

$$T = \sum_{i=1}^{4} T_i = \sum_{i=1}^{4} K_{ti}\omega_i^2 \qquad (19)$$

$$T^B = \begin{bmatrix} 0 \\ 0 \\ T \end{bmatrix} = \begin{bmatrix} 0 \\ 0 \\ T_1 + T_2 + T_3 + T_4 \end{bmatrix} \qquad (20)$$

$$\tau_\phi = K_{t1}\omega_1^2(L - Y_{cg}) - K_{t2}\omega_2^2 Y_{cg} - K_{t3}\omega_3^2(L + Y_{cg}) - K_{t4}\omega_4^2 Y_{cg} \qquad (21)$$

$$\tau_\theta = K_{t1}\omega_1^2 X_{cg} - K_{t2}\omega_2^2(L - X_{cg}) + K_{t3}\omega_3^2 X_{cg} + K_{t4}\omega_4^2(L + X_{cg}) \qquad (22)$$

$$\tau_\psi = K_{d1}\omega_1^2 - K_{d2}\omega_2^2 + K_{d3}\omega_3^2 - K_{d4}\omega_4^2 \qquad (23)$$

Where, $L$ is the distance between the HGAR's GC and the rotation axis of the propeller. The equivalent thrust and drag coefficients $K_{ti}$ and $K_{di}$ can be calculated based on (17) and (18) and using the technical data of the assigned motors and propellers. As in the previous work [16], the selected propeller **CFK** type of 12 inch diameter with a pitch angle of 3.8° has been chosen. This propeller is driven by a brushless DC motor

MK3538 type, which has an electrical power of 350 W. The delivered thrust force of each motor is 2200 gr at propeller speed of 2850 rpm. Finally TABLE I presents these values of $K_{ti}$, $K_{di}$ and the DC motor inertia $I_r$.

### C. Equations of motion

The model of the HGAR is presented in the case of rigid body, the weight of $m_R$ is constant, $m_l$ is the variable, and the center of gravity position is affected by the change of $m_l$ and the position of payload. The value of payload weight is detected by using a force sensor embedded in the gripper. Based on this criteria payload weight is affecting the dynamic model, so $m_l$ is a term added to the total mass of the HGAR. The linear position $\xi = [x \quad y \quad z]^T$ and the orientation $\eta = [\phi \quad \theta \quad \psi]^T$ are expressed in the body frame. The equation of motion is obtained using Newton-Euler equation, and expressed in the inertial frame. The transformation vector which given by (13) is used to transform the fixed body frame to the inertial frame is given by (13).

$$(m_R + m_l)\ddot{\xi} = R_B^I T^B - \dot{\eta} \times m\dot{\xi} - (m_R + m_l)g\hat{Z} - K_{ft}\dot{\xi} \qquad (24)$$

$$I\ddot{\eta} = \tau - \dot{\eta} \times I\dot{\eta} - G_a - K_{fa}\dot{\eta}^2 \qquad (25)$$

Where $K_{ft}$, $K_{fa}$ are the translation drag coefficient and rotational drag coefficient matrices. $G_a$ is the gyroscopic torques due to the rotation of the four rotors. The evaluation of (24) and (25) yields the overall equation of motion.

$$\ddot{x} = \left[ T(c(\psi)s(\theta)c(\phi) + s(\psi)s(\phi)) - K_{ftx}\dot{x} \right]/(m_R + m_l) \qquad (26)$$

$$\ddot{y} = \left[ T(s(\psi)s(\theta)c(\phi) - c(\psi)s(\phi)) - K_{ftx}\dot{y} \right]/(m_R + m_l) \qquad (27)$$

$$\ddot{z} = \left[ T(c(\theta)c(\phi)) - (m_R + m_l)g - K_{ftx}\dot{x} \right]/(m_R + m_l) \qquad (28)$$

$$\begin{bmatrix} \ddot{\phi} \\ \ddot{\theta} \\ \ddot{\psi} \end{bmatrix} = [I]^{-1} \left\{ \begin{bmatrix} \tau_\phi \\ \tau_\theta \\ \tau_\psi \end{bmatrix} - \begin{bmatrix} \dot{\phi} \\ \dot{\theta} \\ \dot{\psi} \end{bmatrix} \times [I] \begin{bmatrix} \dot{\phi} \\ \dot{\theta} \\ \dot{\psi} \end{bmatrix} - \begin{bmatrix} K_{fax} & 0 & 0 \\ 0 & K_{fay} & 0 \\ 0 & 0 & K_{faz} \end{bmatrix} \begin{bmatrix} \dot{\phi}^2 \\ \dot{\theta}^2 \\ \dot{\psi}^2 \end{bmatrix} - I_r \begin{bmatrix} 0 \\ 0 \\ \sum_{i=1}^{4}(-1)^i \omega_i \end{bmatrix} \right\} \qquad (29)$$

Let

$$[J] = \begin{bmatrix} J_{xx} & J_{xy} & J_{xz} \\ J_{yx} & J_{yy} & J_{yz} \\ J_{zx} & J_{zy} & J_{zz} \end{bmatrix} = \begin{bmatrix} I_{xx} & I_{xy} & I_{xz} \\ I_{yx} & I_{yy} & I_{yz} \\ I_{zx} & I_{zy} & I_{zx} \end{bmatrix}^{-1} \qquad (30)$$

For simplifying (29), let $[\tau_x \quad \tau_y \quad \tau_z]^T = [I]^{-1}[\tau_\phi \quad \tau_\theta \quad \tau_\psi]^T$ Then the evaluation of (29) yield to describe the dynamics of the attitude of HGAR.

$$\ddot{\phi} = \tau_x + J_{xz}\left\{ \dot{\phi}\left(I_{yx}\dot{\phi} + I_{yz}\dot{\psi} - I_{yy}\dot{\theta}\right) - \dot{\theta}\left(I_{xz}\dot{\psi} - I_{xx}\dot{\phi} + I_{xz}\dot{\theta}\right) - K_{faz}\dot{\psi}^2 \right\}$$
$$- J_{xz}\left\{ \dot{\psi}\left(I_{yx}\dot{\phi} + I_{yz}\dot{\psi} - I_{yy}\dot{\theta}\right) - \dot{\theta}\left(I_{zx}\dot{\phi} - I_{zz}\dot{\psi} + I_{zy}\dot{\theta}\right) + K_{faz}\dot{\phi}^2 + I_r\dot{\theta}\overline{\Omega} \right\}$$
$$+ J_{xz}\left\{ \dot{\psi}\left(I_{xz}\dot{\psi} - I_{xx}\dot{\phi} + I_{xz}\dot{\theta}\right) - \dot{\phi}\left(I_{zx}\dot{\phi} - I_{zz}\dot{\psi} + I_{zy}\dot{\theta}\right) - K_{fay}\dot{\theta}^2 + I_r\dot{\phi}\overline{\Omega} \right\} \qquad (31)$$

$$\ddot{\theta} = \tau_y + J_{yz}\left\{ \dot{\phi}\left(I_{yx}\dot{\phi} + I_{yz}\dot{\psi} - I_{yy}\dot{\theta}\right) - \dot{\theta}\left(I_{xz}\dot{\psi} - I_{xx}\dot{\phi} + I_{xy}\dot{\theta}\right) - K_{faz}\dot{\psi}^2 \right\}$$
$$- J_{yx}\left\{ \dot{\psi}\left(I_{yx}\dot{\phi} + I_{yz}\dot{\psi} - I_{yy}\dot{\theta}\right) - \dot{\theta}\left(I_{zx}\dot{\phi} - I_{zz}\dot{\psi} + I_{zy}\dot{\theta}\right) + K_{faz}\dot{\phi}^2 + I_r\dot{\theta}\overline{\Omega} \right\}$$
$$+ J_{yy}\left\{ \dot{\psi}\left(I_{xz}\dot{\psi} - I_{xx}\dot{\phi} + I_{xz}\dot{\theta}\right) - \dot{\phi}\left(I_{zx}\dot{\phi} - I_{zz}\dot{\psi} + I_{zy}\dot{\theta}\right) - K_{fay}\dot{\theta}^2 + I_r\dot{\phi}\overline{\Omega} \right\} \qquad (32)$$

1562

$$\ddot{\psi} = \tau_z + J_{zz}\left\{ \dot{\phi}\left(I_{yx}\dot{\phi}+I_{yz}\dot{\psi}-I_{yy}\dot{\theta}\right) - \dot{\theta}\left(I_{xz}\dot{\psi}-I_{xx}\dot{\phi}+I_{xz}\dot{\theta}\right) - K_{faz}\dot{\psi}^2 \right\}$$
$$-J_{zx}\left\{ \dot{\psi}\left(I_{yx}\dot{\phi}+I_{yz}\dot{\psi}-I_{yy}\dot{\theta}\right) - \dot{\theta}\left(I_{zx}\dot{\phi}-I_{zz}\dot{\psi}+I_{zy}\dot{\theta}\right) + K_{faz}\dot{\phi}^2 + I_r\dot{\theta}\overline{\Omega} \right\}$$
$$+J_{zy}\left\{ \dot{\psi}\left(I_{xz}\dot{\psi}-I_{xx}\dot{\phi}+I_{xz}\dot{\theta}\right) - \dot{\phi}\left(I_{zx}\dot{\phi}-I_{zz}\dot{\psi}+I_{zy}\dot{\theta}\right) - K_{fay}\dot{\theta}^2 + I_r\dot{\phi}\overline{\Omega} \right\} \quad (33)$$

Where $\quad \overline{\Omega} = \omega_1 - \omega_2 + \omega_3 - \omega_4 \quad (34)$

The last equations (32 – 34) are derived, assuming that there are small variations in the three angles $\phi$, $\theta$ and $\psi$ such that the corresponding time derivatives of Euler angles are equivalent to the body-fixed angular velocities. From the previous equations of motion four control inputs $\tau_x$, $\tau_y$, $\tau_z$ and $T$ are responsible for achieving the quadrotor movements. These control signals are defined as follows:

$$\begin{bmatrix} T \\ \tau_x \\ \tau_y \\ \tau_z \end{bmatrix} = \begin{bmatrix} 1 & 0 & 0 & 0 \\ 0 & J_{xx} & J_{xy} & J_{xz} \\ 0 & J_{yx} & J_{yy} & J_{yz} \\ 0 & J_{zx} & J_{zy} & J_{zz} \end{bmatrix} \begin{bmatrix} K_{t1} & K_{t2} & K_{t3} & K_{t4} \\ K_{t1}(L-Y_{cg}) & -K_{t2}Y_{cg} & -K_{t3}(L+Y_{cg}) & -K_{t4}Y_{cg} \\ K_{t1}X_{cg} & -K_{t2}(L-X_{cg}) & K_{t3}X_{cg} & K_{t1}(L+X_{cg}) \\ K_{d1} & K_{d2} & K_{d3} & K_{d4} \end{bmatrix} \begin{bmatrix} \omega_1^2 \\ \omega_2^2 \\ \omega_3^2 \\ \omega_4^2 \end{bmatrix}$$
$$(35)$$

## IV. CONTROLLER DESIGN

This section presents the control system design based on the feedback linearization which used to control the attitude and the altitude of the HGAR. The control law is chosen to cancel the nonlinear terms in the equation of motion, and to obtain a good tracking performance. The control laws for the altitude and attitude roll, pitch, and yaw is stated as follows:

$$T = \left((m_R+m_l)U_z + (m_R+m_l)g + K_{ftz}\dot{Z}\right)/(\cos(\phi)\cos(\theta)) \quad (36)$$

$$U_z = \ddot{Z}_d + K_{Zp}e + K_{zd}\dot{e} \quad (37)$$

$$\tau_x = U_\phi - J_{xx}\left\{ \dot{\phi}\left(I_{yx}\dot{\phi}+I_{yz}\dot{\psi}-I_{yy}\dot{\theta}\right) - \dot{\theta}\left(I_{xz}\dot{\psi}-I_{xx}\dot{\phi}+I_{xz}\dot{\theta}\right) - K_{faz}\dot{\psi}^2 \right\}$$
$$+J_{xz}\left\{ \dot{\psi}\left(I_{yx}\dot{\phi}+I_{yz}\dot{\psi}-I_{yy}\dot{\theta}\right) - \dot{\theta}\left(I_{zx}\dot{\phi}-I_{zz}\dot{\psi}+I_{zy}\dot{\theta}\right) + K_{faz}\dot{\phi}^2 + I_r\dot{\theta}\overline{\Omega} \right\}$$
$$+J_{xz}\left\{ \dot{\psi}\left(I_{xz}\dot{\psi}-I_{xx}\dot{\phi}+I_{xz}\dot{\theta}\right) - \dot{\phi}\left(I_{zx}\dot{\phi}-I_{zz}\dot{\psi}+I_{zy}\dot{\theta}\right) - K_{fay}\dot{\theta}^2 + I_r\dot{\phi}\overline{\Omega} \right\} \quad (38)$$

$$U_\phi = \ddot{\phi}_d + K_{\phi p}e + K_{\phi d}\dot{e} \quad (39)$$

$$\tau_y = U_\theta - J_{yz}\left\{ \dot{\phi}\left(I_{yx}\dot{\phi}+I_{yz}\dot{\psi}-I_{yy}\dot{\theta}\right) - \dot{\theta}\left(I_{xz}\dot{\psi}-I_{xx}\dot{\phi}+I_{xy}\dot{\theta}\right) - K_{faz}\dot{\psi}^2 \right\}$$
$$+J_{yx}\left\{ \dot{\psi}\left(I_{yx}\dot{\phi}+I_{yz}\dot{\psi}-I_{yy}\dot{\theta}\right) - \dot{\theta}\left(I_{zx}\dot{\phi}-I_{zz}\dot{\psi}+I_{zy}\dot{\theta}\right) + K_{faz}\dot{\phi}^2 + I_r\dot{\theta}\overline{\Omega} \right\}$$
$$-J_{yy}\left\{ \dot{\psi}\left(I_{xz}\dot{\psi}-I_{xx}\dot{\phi}+I_{xz}\dot{\theta}\right) - \dot{\phi}\left(I_{zx}\dot{\phi}-I_{zz}\dot{\psi}+I_{zy}\dot{\theta}\right) - K_{fay}\dot{\theta}^2 + I_r\dot{\phi}\overline{\Omega} \right\} \quad (40)$$

$$U_\theta = \ddot{\theta}_d + K_{\phi p}e + K_{\phi d}\dot{e} \quad (41)$$

$$\tau_z = U_\psi - J_{zz}\left\{ \dot{\phi}\left(I_{yx}\dot{\phi}+I_{yz}\dot{\psi}-I_{yy}\dot{\theta}\right) - \dot{\theta}\left(I_{xz}\dot{\psi}-I_{xx}\dot{\phi}+I_{xz}\dot{\theta}\right) - K_{faz}\dot{\psi}^2 \right\}$$
$$-J_{zx}\left\{ \dot{\psi}\left(I_{yx}\dot{\phi}+I_{yz}\dot{\psi}-I_{yy}\dot{\theta}\right) - \dot{\theta}\left(I_{zx}\dot{\phi}-I_{zz}\dot{\psi}+I_{zy}\dot{\theta}\right) + K_{faz}\dot{\phi}^2 + I_r\dot{\theta}\overline{\Omega} \right\}$$
$$+J_{zy}\left\{ \dot{\psi}\left(I_{xz}\dot{\psi}-I_{xx}\dot{\phi}+I_{xz}\dot{\theta}\right) - \dot{\phi}\left(I_{zx}\dot{\phi}-I_{zz}\dot{\psi}+I_{zy}\dot{\theta}\right) - K_{fay}\dot{\theta}^2 + I_r\dot{\phi}\overline{\Omega} \right\} \quad (42)$$

$$U_\psi = \ddot{\psi}_d + K_{\phi p}e + K_{\phi d}\dot{e} \quad (43)$$

where $K_p$ and $K_d$ are the proportional and differential controller gains respectively. These gains are selected to obtain a satisfied controller performance. Table III presents the controller parameters. The control of X and Y movements are based on the controlling of $\theta$ and $\phi$ respectively. Nonholonomic constraints are defining the coupling between all the previous states. The nonholonomic constraints are used to generate the desired trajectory for $\theta$ and $\phi$, which will satisfies the control of the X and Y movements.

$$\tan(\phi) = \frac{(m\ddot{x}+K_{ftx}\dot{x})\cos(\psi)+(m\ddot{y}+K_{fty}\dot{y})\sin(\psi)}{(m\ddot{z}+K_{ftz}\ddot{z}+mg)} \quad (44)$$

$$\sin(\theta) = \frac{(m\ddot{x}+K_{ftx}\dot{x})\sin(\psi)-(m\ddot{y}+K_{fty}\dot{y})\cos(\psi)}{\sqrt{(m\ddot{x}+K_{ftx}\dot{x})^2+(m\ddot{y}+K_{fty}\dot{y})^2+(m\ddot{z}+K_{fty}\dot{z}+mg)^2}} \quad (45)$$

## V. TRANSFORMATION MECHANISM

### A. Modeling and analysis

Fig. 5 presents a schematic drawing for the transformation mechanism. This mechanism is driven through an arbitrary rotational angle $\varphi$ as a result of the generated thrust force by propeller. Unlike the traditional mechanical systems which are rotated by applying a torque directly to the linkage joint. The torque required to the rotor arm is produced by the resultant force which generated by the competing effect of the thrust force, T, and the gravitational weight. Different gravitational forces are applied to the rotor arm; first one is the weight of the brushless DC motor $W_1$ and its effect point at a distance $L_1$. $W_2$ is the second force and denoted for the arm weight and its effect at $L_2$. Finally $W_3$ and $W_4$ are the weights of the solenoids which used to secure the rotor arm into its position. These forces affect points at $L_3$ and $L_4$. The operating range for the transformation mechanism is specified as 0- 90°. The dynamics of the transformation mechanism can be expressed using Newton's law in the following differential equation:

$$J_{arm}\ddot{\varphi} = T_iL_1 - (W_1L_1+W_2L_2+W_3L_3+W_4L_4)\cos\varphi \quad (46)$$
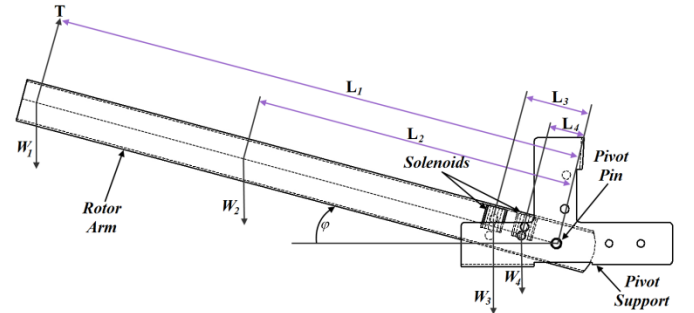
Figure 5. SCHEMATIC DRAWING FOR TRANSFORMATION MECHANISM'S FORCES

### B. Controller Design

Since the mathematical model for the transformation mechanism is established in (47). A model based controller is designed based on the feedback linearization technique. The control law which regulate the movement of the rotor arm is presented as follow:

$$T_i = \left(J_{arm}U_\varphi + (W_1L_1+W_2L_2+W_3L_3+W_4L_4)\cos(\varphi)\right)/L \quad (47)$$

$$U_\varphi = \ddot{\varphi}_d + K_{\varphi p}e + K_{\varphi d}\dot{e} \quad (48)$$

1563

A fifth order polynomial trajectory for $\varphi$ and $\dot\varphi$ has been generated to be used as a reference signal to the rotor arm.

## VI. SIMULATION RESULTS

In order to implement the derived dynamic model and the control system, a simulation model has been developed. The HGAR model using the parameter in Table III is implemented in MATLAB/SIMULINK for simulation. A fifth order polynomial trajectories is generated and used as a reference trajectory for $z, \phi, \theta$ and $\psi$. From the simulation results in Fig.6, 7, 8, 10, 11 and 12 one can notice that the measured trajectory is tracking the desired trajectory, and it has a zero error. Fig.9 presents the angular speeds of all the rotors and these values are not equal. The values of angular speed of rotors 1 and 2 are the highest because their position near to the CM. Finally, from Fig.13, 14 good tracking of the transformation mechanism for the reference signal.

TABLE III.
CONTROLLER GAINS

| Parameter | $K_p$ | $K_d$ |
|---|---|---|
| Roll | 11 | 5 |
| Pitch | 10 | 7 |
| Yaw | 0.5 | 0.003 |
| Altitude | 10 | 5 |
| Transformation Mechanism | 10 | 25 |



Figure 6. TRAJECTORY RESPONSE FOR THE ALTITUDE
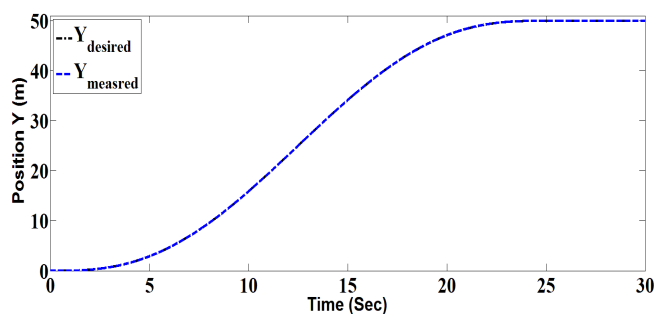


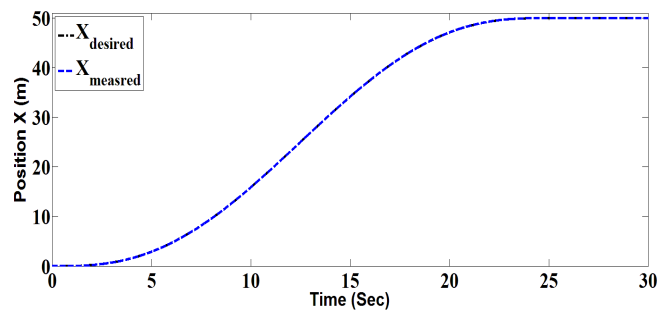Figure 7. TRAJECTORY RESPONSE FOR THE Y-AXIS POSITION



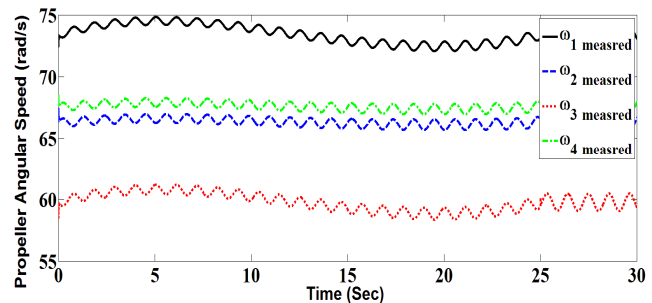Figure 8. TRAJECTORY RESPONSE FOR THE X-AXIS POSITION



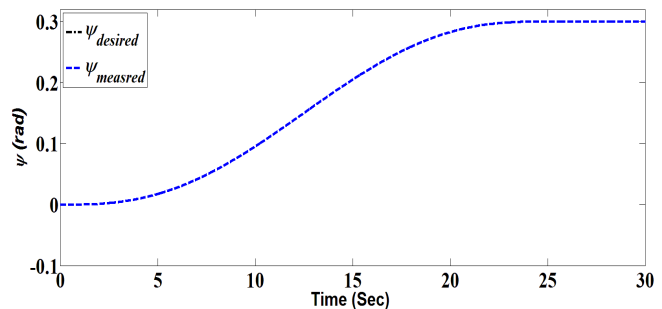Figure 9. THE ANGULAR SPEEDS OF ALL THE ROTORS



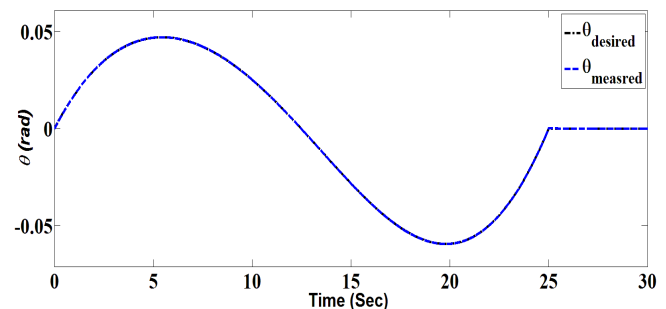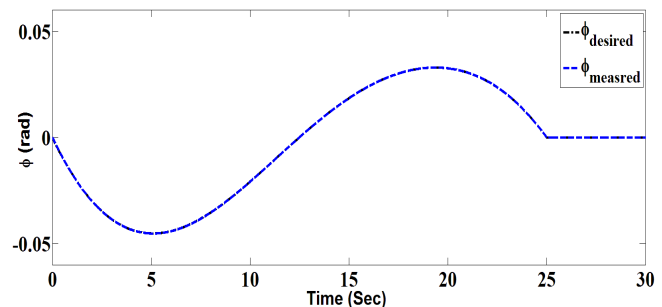Figure 10. TRAJECTORY RESPONSE FOR THE YAWING ANGLE
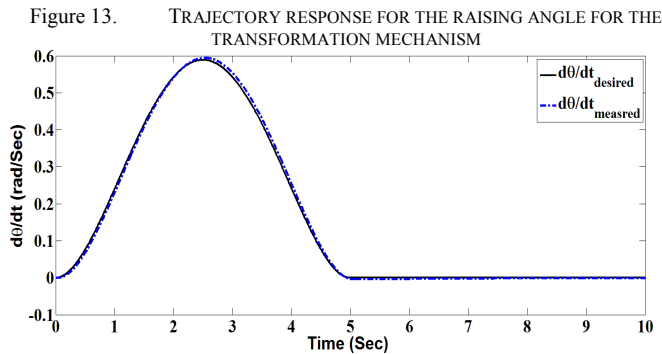


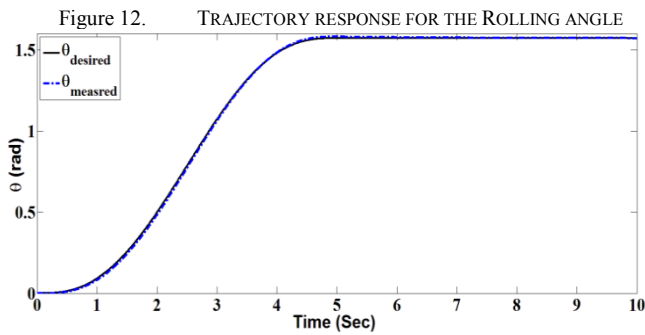Figure 11. TRAJECTORY RESPONSE FOR THE PITCHING ANGLE



1564

Figure 12.    TRAJECTORY RESPONSE FOR THE ROLLING ANGLE

Figure 13.    TRAJECTORY RESPONSE FOR THE RAISING ANGLE FOR THE
TRANSFORMATION MECHANISM

Figure 14.    TRAJECTORY RESPONSE FOR THE RAISING ANGLUR VELOCITY
FOR THE TRANSFORMATION MECHANISM

## VII. CONCLUSION

In this paper a novel Hybrid Ground Aerial Robot (HGAR) has been presented to satisfy its goal to move on ground and vertically take off to fly. The key feature of this robot is the simplicity and efficiency of the transformation mechanism that switches between the ground and the flying motion configurations without adding any additional actuators. A direct relationship between the payload and all the robot physical parameters such as the position of the center of mass and mass moment of inertia is established. The dynamic model of robot has derived. The eccentricity problem which caused from the shift of the center of gravity away from the geometric center is handled and resolved in the dynamic model. The dynamic model takes into account the effect of the payload which handled using the manipulator during the ground motion configuration. Controller is designed based on the feedback linearization technique and using the nonholonomic constraints. A high order polynomial trajectory is generated to be used as a reference signal to X, Y, Z and ψ. The simulation results show that the controller is tracking the desired trajectory based on the payload mass and canceling the nonlinear terms. For future work, building a robust controller for this robot is needed to deal with the uncertainty of changing the payload. An algorithm will be built to estimate the mass of the payload. Also, the dynamic model will be completed for HGAR in ground motion configuration. Finally experimental setup for the proposed new robot will be carried out.

## REFERENCES

[1]    S. A. Moosavian, H. Semsarilar, A. Kalantari, " Design and Manufacturing of a mobile rescue robot" IEEE/RSJ international conference on intelligent Robots and Systems, Beijing, China, pp. 3982-3987, Oct. 2006.

[2]    R. Siegwart, and I.R. Nourbakhsh, "Introduction to Autonomous Mobile Robots", MIT press, 2004.

[3]    Kimon P. Valavanis, "Advances in Unmanned Aerial Vehicles", Springer, 2007.

[4]    P. Castillo, R. Lozano, and A. Dzul, " Modeling and Control of Mini-Flying Machines", Springer, 2005.

[5]    K. Nonami, F. Kendoul, S. Suzuki, W. Wang, D. Nakkazawa, " Autonomous Flying robots ", Springer, 2010.

[6]    C. Bermes, S. Bouabdallah, D. Schafroth, R. Siegwart, " Design of the autonomous micro helicopter muFly", Int. Journal of Mechatronics, Vol. 21, pp. 765-775, 2011.

[7]    P. Pounds, and R. Mahony, "Design Principles of Large Quadrotors for Pratical Applications", IEEE international Conference on Robotics and Automation, Kobe, Japan, pp. 3265-3270, May 2007.

[8]    Y. Naidoo, R. Stopforth, G. Bright, " Rotor Aerodynamic Analysis of a Quadrotor for thrust Critical Applications", Robotics and Mechatronics conference (ROBMECH), Pretoria, South Africa, Nov., 2011.

[9]    B. Erginer, and E. Altug, "Modelling and PD Control of a Quadrotor VTOL Vehicle" IEEE Intelligent Vehicles Symposium, Istanbul, Turkey, pp. 894-899, June, 2007.

[10]    H. Huang, G. M. Hoffmann, S. L. Waslander, C. J. Tomlin, " Aerodynamics and control of Autonomous Quadrotor Helicopters Aggressive Maneuvering", IEEE international Conference on Robotics and Automation, Kope, Japan, pp. 3277-3282, May 2009.

[11]    S. Bouabdallah, and R. Siegwart, "Full Control of a Quadrotor", IEEE/RSJ Conference on intelligent Robots and Systems, San Diego, CA, USA, pp. 153-158, Oct 2007.

[12]    A. Tayebi and S. McGilvray, " Attitude Stablization of a VTOL Quadrotor Aircraft" IEEE Trans. On Control Systems Technology, VOL.14, NO.3, pp. 562- 571, MAY 2006.

[13]    J. Kim, M. Kang, S. Park, "Accurate Modeling and Robust Hovering Control for a Quad–rotor VTOL Aircraft," J Intell Robot Syst 2010.

[14]    M. Heidarian and A. memon, " Attitude Control of VTOL-UAVs" UKACC International Conference on Control, Cardiff, UK, pp. 363-368, September, 2011

[15]    J. Li and Y. Li, "Dynamic Analysis and PID Control Control for a Quadrotor", IEEE International Conference on Mechatronics and Automation, Beijing, China, pp. 573-578, August 2011.

[16]    M. Elsamanty, M. Fanni and A. Ramadan, "Novel Hybrid Ground/Aerial Autonomous Robot" 1st International Conference on Innovative Engineering Systems (IEEE-RAS ICIES2012), Dec. 7-9, Egypt, 2012.

[17]    D. Mellinger, Q. Lindsey, M. Shomin, and V. Kumar, "Design, Modeling, Estimation and Control for Aerial Grasping and Manipulation," IEEE/RSJ International Conference on Intelligent Robots and Systems San Francisco, CA, USA, September 25-30, 2011.

[18]    A. Khalifa, M. Fanni, A. Ramadan and A. Abo- Ismail, "Modeling and Control of a New Quadrotor Manipulation System" 1st International Conference on Innovative Engineering Systems (IEEE-RAS ICIES2012), Dec. 7-9, Egypt, 2012.

[19]    T. Raharijaona and F. Batemen, "Robust Control for an off centered Quadrotor"19th Mediterranean Conference on Control and Automation, Corfu, Greece, pp. 1253-1258, June 2011.